Journal of Alloys and Compounds 739 (2018) 653–659

Contents lists available at ScienceDirect

Journal of Alloys and Compounds

journal homepage: http://www.elsevier.com/locate/jalcom

Effect of supersonic spraying impact velocity on opto-electric properties of transparent conducting flexible films consisting of silver nanowire, ITO, and polyimide multilayers

Tae-Gun Kim [a, 1], Jong-Gun Lee [a, 1], Chan-Woo Park [a], Hong-Seok Jo [a], Min-Woo Kim [a], Maikel F.A.M. van Hest [b], Dae-Hyung Cho [c], Yong-Duck Chung [c, **], Sam S. Yoon [a, *]

[a] School of Mechanical Engineering, Korea University, Seoul 02841, Republic of Korea
[b] National Renewable Energy Laboratory, Golden, CO 80401, USA
[c] Electronics and Telecommunications Research Institute (ETRI), 218 Gajeong-ro, Yuseong-gu, Daejeon 34129, Republic of Korea

ARTICLE INFO

Article history:
Received 16 October 2017
Received in revised form
13 December 2017
Accepted 22 December 2017
Available online 26 December 2017

Keywords:
Supersonic spray
Self-fusion
Silver nanowires
Transparent conducting film
Flexible substrate

ABSTRACT

We demonstrate the use of supersonic spraying for the deposition of silver nanowires (AgNWs) on a flexible polyimide (PI) substrate for the formation of transparent and conducting films (TCF) as an alternative to nonflexible ITO (indium tin oxide). The self-fused intersections of the NWs resulted in films with a low sheet resistance (R_s = 31 Ω/sq) and fairly high transmittance (Tr = 92%) on a glass substrate. The effect of the impact speed of the supersonically sprayed AgNWs on the opto-electric properties of the flexible TCF was evaluated by varying the spray coating conditions. The fabricated films were characterized by X-ray diffraction analysis, atomic force microscopy, ultraviolet–visible spectroscopy, and scanning electron microscopy. Finally, cyclic bending tests were performed on the PI/AgNW films as well as PI/ZnO/indium tin oxide/AgNW films, and the changes in their electrical properties with bending were compared.

1. Introduction

Polyimide (PI) substrates have been proposed as flexible alternatives for various applications [1–3]. The performance of thin film solar cells based on PI substrates remains stable, with the cells showing high flexibility, even under severe mechanical stress [4]. Compared to flexible stainless steel substrates, PI substrates are more beneficial because of their electrically insulating nature, which allows for the formation of direct interconnections and thus a decrease in the production costs [5,6].

However, even in the case of flexible PI substrates, challenges remain owing to the brittleness of the indium tin oxide (ITO) layer that must be deposited on the substrate to enable electrical conduction. ITO shows good mechanical and chemical stabilities and is a suitable transparent electrode material for next-generation opto-electronic devices, owing to its relatively low sheet resistance and high transmittance [7]. However, it is brittle and therefore cannot be used in flexible and stretchable devices [8]. For these reasons, one- or two-dimensional materials such as carbon nanotubes (CNTs) [9,10], metal nanowires (NWs) [11,12], and graphene [13,14] have been suggested as alternative transparent electrode materials, because these materials are highly conductive and transparent and exhibit desirable characteristics owing to their nanoscale dimensions. For instance, their nanoscale dimensions allow them to exhibit high light transmittance.

These nanomaterials can be deposited via various nonvacuum-based coating methods, such as drop casting [15,16], vacuum filtration [17], and spin coating [11,18]. Drop casting involves depositing a solution of the nanomaterial onto the substrate and subjecting the solution-coated substrate to drying, during which the Marangoni or/and coffee-ring effect can occur and cause nonuniformities in the coating [19]. Methods such as vacuum filtration allow for the formation of NWs on glass, polydimethylsiloxane, and polyethylene terephthalate substrates. However, it is difficult to use the vacuum filtration method for large-area deposition; therefore, it is not suitable for commercial purposes [20]. On the other hand,

* Corresponding author.
** Corresponding author.
E-mail addresses: ydchung@etri.re.kr (Y.-D. Chung), skyoon@korea.ac.kr (S.S. Yoon).
[1] These authors have contributed equally.

https://doi.org/10.1016/j.jallcom.2017.12.237
0925-8388/

spin coating allows for the rapid fabrication of NWs on substrates. However, much of the costly precursor is wasted during the spinning process. Further, the method is not extendable for large-area synthesis [20,21]. Finally, all these methods require a post-deposition thermal treatment to evaporate the precursor solution, which adds to the overall fabrication cost [22].

Lee et al. [23] proposed a supersonic spraying method to deposit silver NWs (AgNWs). This method is rapid and scalable and does not require the use of a vacuum. As a result, it does not exhibit any of the abovementioned shortcomings of the conventional methods. Furthermore, supersonic spraying results in self-fusion at the intersections of the deposited NWs, owing to the high impact speed; this eliminates the need for postdeposition processing (such as pressing or a thermal treatment) for fusing the NW intersections [24]. It has been shown that the high contact resistance of unfused NWs lowers the overall performance of the resulting transparent and conducting films [25].

In this study, we used supersonic spraying to fabricate transparent and conducting films of AgNWs on flexible PI substrates together with an ITO layer of various thickness as a window layer for potential application in flexible solar cells, which has not been previously attempted. Therefore, multilayers of ZnO/ITO/AgNW are considered herein. In addition, the electrical and mechanical properties of the multilayer films are evaluated and compared. The optimal spraying condition that produces the lowest sheet resistance and high transmittance is identified.

2. Materials and methods

2.1. Supersonic spraying of AgNWs

Fig. 1 shows a schematic of the supersonic spray-coating method. Compressed air was heated through an air heater, and its velocity was increased to the supersonic range by making it pass through the nozzle. The pressure (P_0) and temperature (T_0) ranges at which the velocity of the heated air corresponded to the supersonic range were found to be $4 \leq P_0 \leq 6$ bar and $60 < T_0 < 220$ °C, respectively (see Table 1). PI films (50 μm in thickness, Upilex, Ube Industries Ltd., Japan) and slide glass were used as the substrates.

ZnO (70 nm) and ITO layers were deposited by radiofrequency (RF) magnetron sputtering in Ar/O_2 and pure Ar gas, respectively.

Table 1
Operating conditions for supersonic spray coating.

Conditions	
Pressure [bar]	4–6
Gas preheating temperature [°C]	60–220
Flow rate [ml/min]	1.2
Nozzle to substrate distance [mm]	180

During ZnO deposition, the temperature of the substrate, power for RF sputtering, Ar/O_2 flowrate, and deposition pressure were room temperature, 100 W, 30/10 sccm, and 4.0 Pa, respectively. To deposit the ITO film, a sintered ceramic target (99.99%, $In_2O_3/SnO_2 = 90:10$ (wt%)) with a diameter of 10.1 cm was used. The target-to-substrate distance was approximately 20 cm. For the ITO sputter deposition process, an RF power of 100 W, Ar flow of 50 sccm, and operating pressure of 0.67 Pa were used. ITO films with thicknesses of 50 and 150 nm were deposited at a growth temperature (T_G) of 200 °C [26].

The AgNWs to be deposited, which were dispersed in isopropyl alcohol (IPA, Duksan, Korea) at a concentration 0.15 wt%, had an average diameter and length of 20 nm and 15 μm, respectively. The AgNW dispersion was diluted further using IPA to an IPA/AgNW ratio of 2:1. Next, the AgNW dispersion was supplied to an ultrasonic atomizer (VCX, 40 kHz, Sonics & Materials, USA) at a flowrate of 1.2 mL/min using a syringe pump (Legato 210, KDS, USA). The AgNW dispersion was made to flow from the atomizer into the supersonic stream of heated air in the form of atomized droplets, resulting in the rapid evaporation of the IPA dispersant. This left behind dried AgNWs, which fused and formed a coating on the substrate.

2.2. Film characterization

The crystallinities and crystal phases of the fabricated films were characterized by X-ray diffraction (XRD) analysis (SmartLab, Rigaku, Japan), which was performed using Cu-Kα radiation for 2θ values of 10–70°. The surface roughnesses and morphologies of the films were observed using atomic force microscopy (AFM) (XE-100, Park Systems, Korea) and field-emission scanning electron microscopy (FE-SEM) (S-5000, Hitachi, Ltd.), respectively. Finally, the optical properties of films were evaluated using an

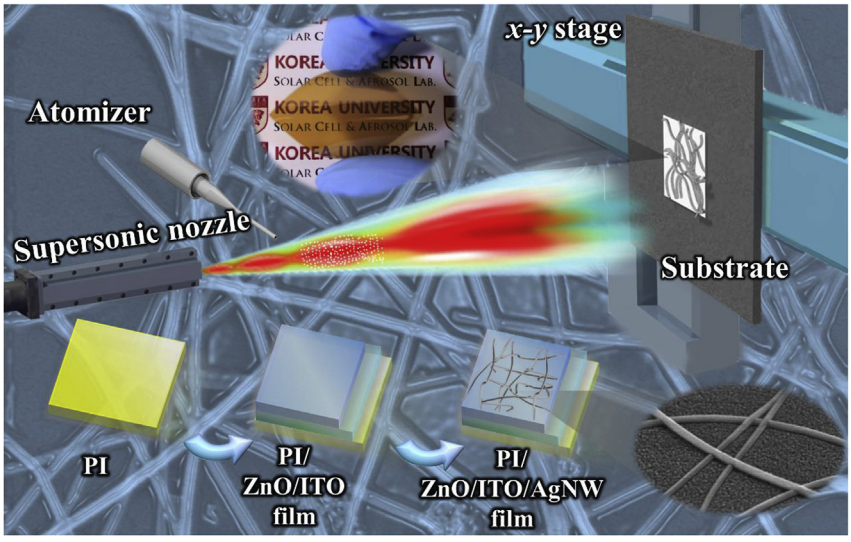

Fig. 1. Schematic of supersonic spraying for depositing precursor of AgNWs on PI-based substrates. Bottom inset in the right corner shows self-fusion of nanowire intersections, and top inset shows the flexible PI substrate.

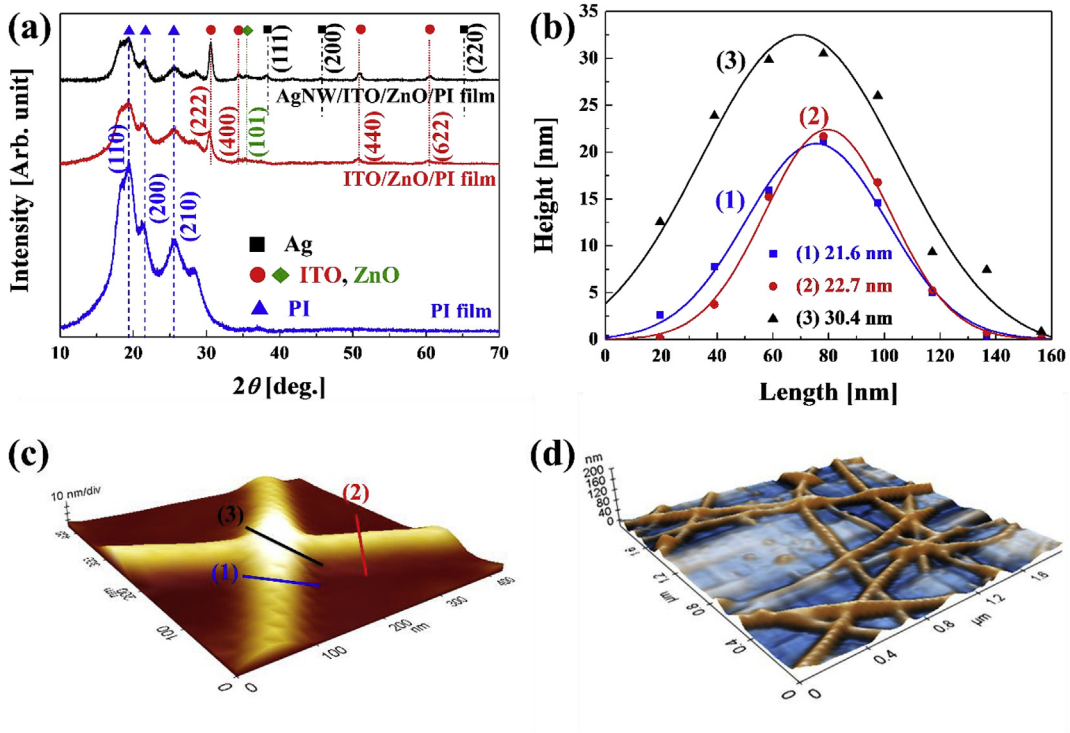

Fig. 2. (a) XRD patterns of PI substrate, ITO/ZnO/PI substrate, and AgNW/ITO/ZnO/PI substrate. (b) Height–length graph (c) and (d) AFM images.

ultraviolet–visible (UV–vis) spectrophotometer (Lambda 650S, Perkin Elmer, USA).

3. Results and discussion

Fig. 2a shows the XRD patterns of the bare PI, ITO/ZnO-coated PI, and AgNW/ITO/ZnO-coated PI substrates. In the case of the bare PI substrate (blue line), the main diffraction peaks are observed in the 10–70° range and are related to the (110), (200), and (210) planes of the crystalline Upilex-S PI substrate [27]. On the other hand, the XRD pattern of the ITO/ZnO/PI substrate (red line) contains peaks at 30.4°, 35.2°, 50.8°, and 60.4°; these correspond to the (222), (400), (440), and (622) planes of ITO. Further, the peak at 35.5° is attributable to the (101) plane of ZnO [28,29]. The XRD pattern of the AgNW/ITO/ZnO/PI substrate is represented by the black line. Based on the JCPDS #04-0783 card, the peaks at 38.1°, 45.4°, and 65.1° could be assigned to the (111), (200), and (220) planes, respectively, of fcc-structured Ag.

Fig. 2b shows the height of the intersection between the AgNWs, which is approximately 30 nm, whereas the diameter of the AgNWs is approximately 20 nm; this suggests that the AgNWs formed partial junctions. Fig. 2c and d shows magnified AFM images of the intersecting AgNWs quantified in Fig. 2b. The junctions formed on the surface of the AgNW/ITO/ZnO/PI sample were analyzed using cross-sectional SEM (not shown). The maximum NW height did not exceed 40 nm; this was true even in the area where several AgNWs overlapped. Further, the multiple overlapping NWs formed a net-like structure, by which the deposited AgNW films exhibited high transmittance and low sheet resistance.

Fig. 3 shows the UV–vis transmittance values of the AgNW films coated on slide glass substrates at different inlet air temperatures (T_0) and pressures (P_0). Because the PI substrate has its own color, slide glass was used to measure the transmittance of the AgNW layer for these parametric studies. The deposition pressure ranged from 4 bar to 6 bar, whereas the temperature ranged from 60 °C to 220 °C, as shown in the figure. Lee et al. [30] used the isentropic flow equation to estimate the gas exit velocity at the nozzle:

$$V_e = \sqrt{2c_p T_0 \left(1 - \frac{P_e}{P_0}\right)^{\frac{\gamma-1}{\gamma}}} \quad (1)$$

where c_p is the specific heat, and T_0 and P_0 are the stagnation temperature and pressure, respectively, of the carrier gas. A specific heat ratio of $\gamma = 1.4$ was used. Here, P_e is the nozzle exit pressure, which was taken to be atmospheric pressure; that is, $P_e = P_{atm}$. Therefore, if P_0 or T_0 were to increase, the gas exit velocity, V_e, would correspondingly increase. The isentropic velocity for $P_0 = 4$, 5, and 6 bar was 793–965 m/s, 798–971 m/s, and 801–975 m/s, respectively, for a change in the stagnation temperature (T_0) from 60 °C to 220 °C. Equation (1) also indicates that the effect of P_0 on V_e was almost negligible, whereas the effect of T_0 on V_e was relatively significant. Fig. 3a–c show that greater transmittance was achieved for all P_0 values when a higher T_0 was used. However, this transmittance increase was not accomplished without sacrificing the sheet resistance, as indicated in Fig. 3d.

Fig. 3d shows the transmittance versus sheet resistance data for the films fabricated at various P_0 values. The record of the interest is marked at $R_s = 31$ Ω/sq and $Tr = 92\%$ acquired from $P_0 = 4$ bar; compare these values with the ones in Table 2. As expected, the sheet resistance increased with increasing transmittance. These films with different transmittances were fabricated not by varying the deposition time but by changing the deposition temperature, T_0. The increased transmittance (Tr) in Fig. 3d corresponds to an increase in T_0 for all values of pressure, P_0. At a lower sheet resistance ($R_s < 15$ Ω/sq), the effect of P_0 was insignificant. However, it is clear that the films produced at $P_0 = 4$ bar exhibited higher transmittance than those deposited at higher pressure for a similar R_s. At higher P_0 values, it was difficult to achieve transmittance greater than 92% without sacrificing R_s. The sheet resistance

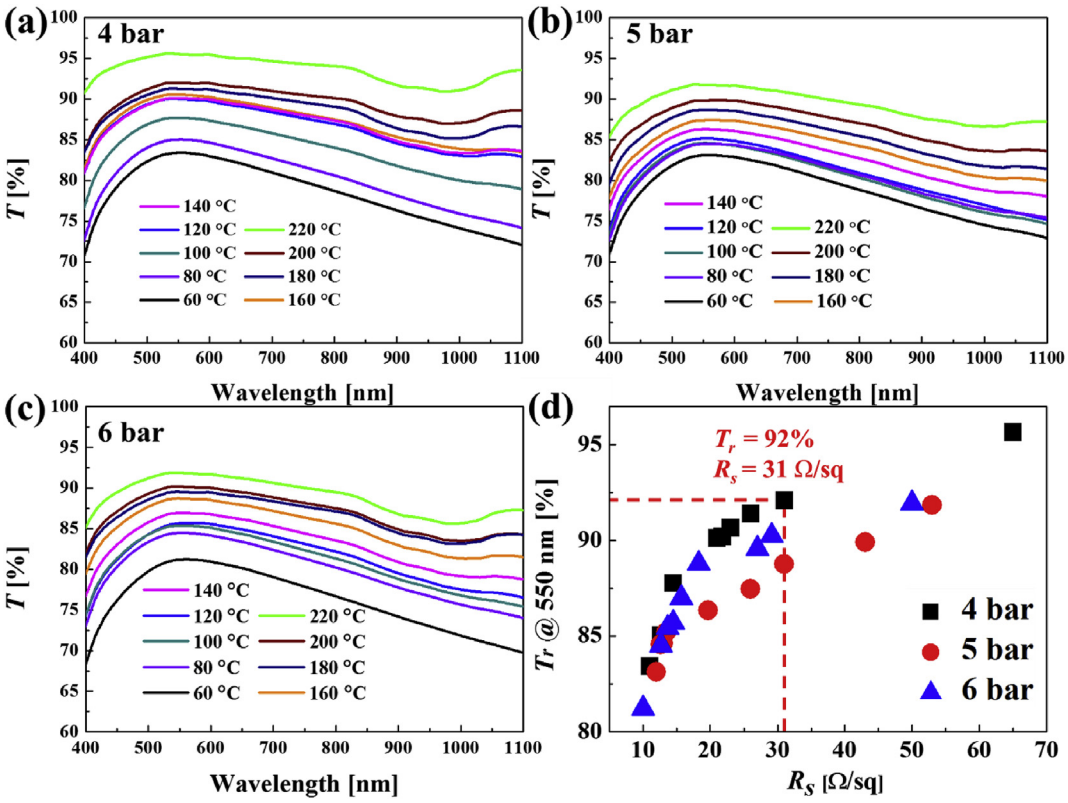

Fig. 3. Transmittances of films produced at deposition pressure, P_0, of (a) 4 bar, (b) 5 bar, and (c) 6 bar. (d) Transmittance (Tr) versus sheet resistance (R_s) values for different P_0 values.

Table 2
Comparison of the sheet resistance and transmittance from existing literature against our present value.

Materials	T_r [%]	R_s [Ω/sq]	Ref.
AgNW	92	14	[23]
Graphene	92	70	[36]
AgNW	87.5	92	[37]
PEDOT: PSS	93	156	[23]
SWNT	90.4	330	[38]

increased rapidly to the range of 50 Ω/sq when $Tr > 92\%$. The higher R_s at higher T_0 was due to fewer NWs deposited on the substrate. At high T_0, the air stream velocity exiting from the supersonic nozzle also increased according to Eq. (1), which produced accumulation shockwaves at the colliding substrate. As a result, light materials such as NWs were bounced by the accumulated shockwaves at the substrate and deviated from the deposition trajectories [31–33].

Fig. 4 compares figure of merit (FoM) values of the films fabricated at different P_0 and T_0 values. Haacke suggested a simple expression for the FoM—namely, $\text{FoM} = Tr^n/R_s$; here, n values of 5, 10, 20, and 100 correspond to Tr values of 85, 90, 95, and 99%. The optimal film thickness—that is, the thickness for which the FoM is highest—is defined as $d_{opt} = 1/(n \cdot \alpha)$, where α is the absorption coefficient.

It can be seen that the FoM decreased with increasing T_0 for n values of 5 and 10. On the other hand, FoM increased with increasing T_0 for n values of 20 and 100. This reversed pattern implies that FoM changes depending on where the focus of the interest is placed in producing transparent conducting films. For example, if one is interested in producing relatively low-transmittance film ($Tr < 90\%$), then the spraying operating condition for T_0 should be kept low because FoM is highest when T_0 is lowest. On the other hand, if one is interested in producing relatively high-transmittance films ($Tr > 95\%$), then the spraying operating condition for T_0 should be kept high because FoM is highest when T_0 is highest.

The effect of P_0 appears to be minor for $n = 5$ in Fig. 4a. Overall, $P_0 = 4$ bar tended to produce films with greater FoM for the remaining cases of $n = 10$, 20, and 100. The opto-electric properties of the films produced at lower operating pressure (P_0) tended to perform well. This pattern was especially clear at higher $n = 20$ and 100. Thus, it is safe to conclude that $P_0 = 4$ bar was the optimal coating condition.

Fig. 5 shows the effect of T_0 on the surface morphology of the deposited AgNW films. The deposition pressure, P_0, was fixed at 6 bar. The area occupied by the AgNWs was estimated from the SEM images shown in figure. As expected, fewer AgNWs were deposited at higher T_0 values, owing to the "bow shock" effect generated at the air-colliding substrate [31–33]. The area covered by the AgNWs changed from 75% to 19% when the deposition temperature, T_0, was increased from 60 °C to 160 °C. The effect of T_0 on the exit velocity, V_e, was pronounced. When V_e was increased, the expansion waves bounced against the nozzle walls and created shockwaves that traveled downstream. These shockwaves collided with the substrate, increasing the pressure at the impact region and resulting in what is known as bow shock [31–33]. This bow shock effect has been observed in numerous experimental studies and numerical simulations. Smaller objects (such as NWs) are readily influenced by bow shock, which deflects the incoming materials, thus preventing them from being deposited. Unfortunately, there is no straightforward way to prevent bow shock without controlling the deposition velocity. Thus, the only way to overcome the adverse effects of bow shock is to deposit heavy materials at a high impact

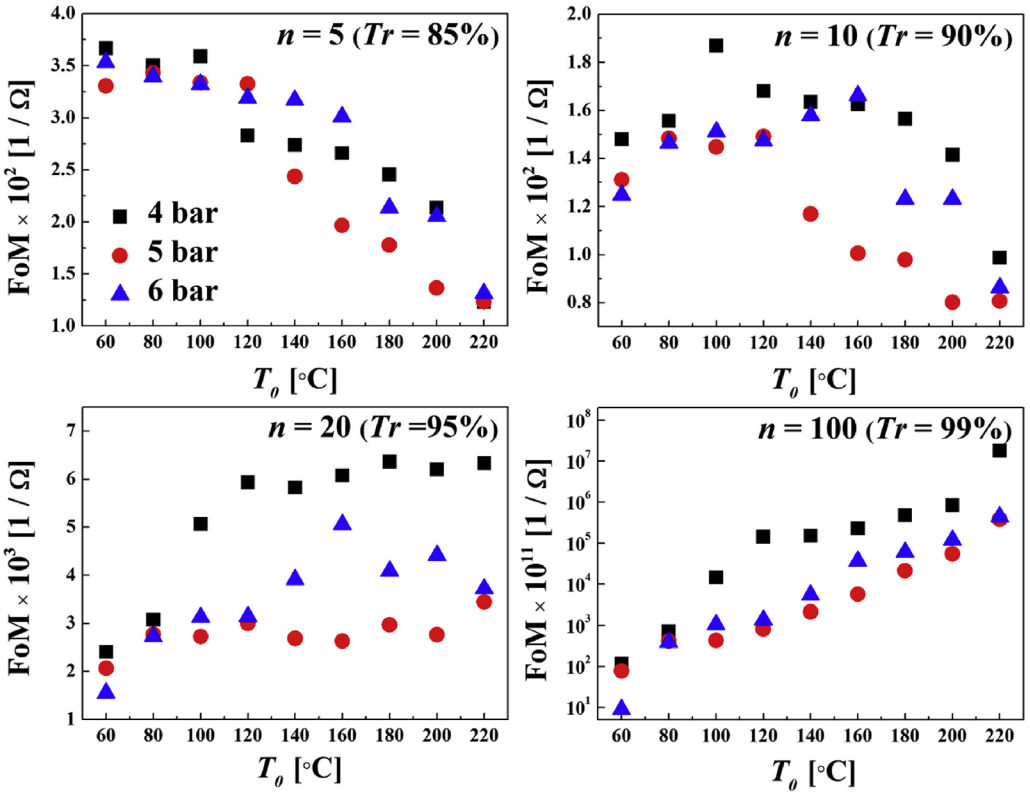

Fig. 4. Haacke's figure of merit (FoM) ($= Tr^n/R_s$) for n values of 5, 10, 20, and 100, which correspond to Tr values of 85, 90, 95, and 99%.

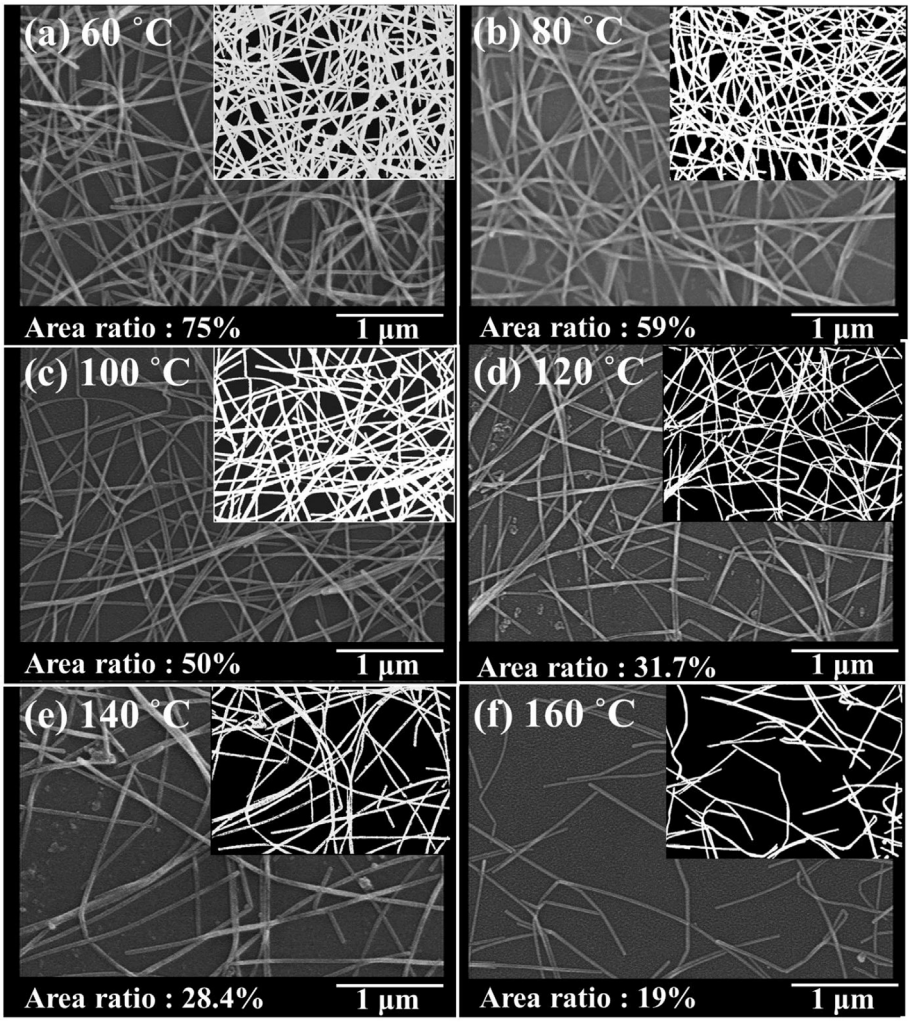

Fig. 5. SEM images of AgNWs deposited on glass substrates at 60 °C ≤ T_0 ≤ 160 °C and a constant deposition pressure, P_0, of 6 bar.

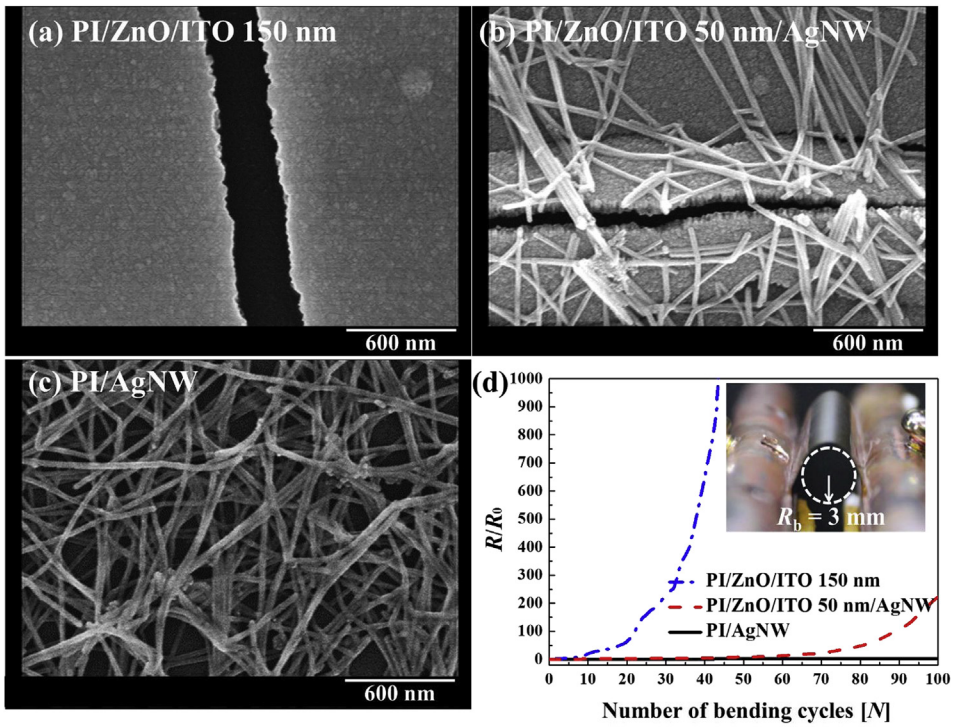

Fig. 6. SEM images of (a) PI/ZnO/ITO (150 nm) sample after $N = 7$ bending cycles, (b) PI/ZnO/ITO (50 nm)/AgNW sample after $N = 50$ bending cycles, and (c) PI/AgNW sample after $N = 2000$ bending cycles. (d) Sheet resistance variation of the films after the bending cycle tests.

velocity, which allows the materials to penetrate the bow shock-wave and be deposited onto the substrate regardless of the bow shock. However, lighter materials such as NWs are readily deflected by the bow shock at the substrate, and the only way to deposit such materials efficiently is to reduce the impact velocity and prevent the bow shock phenomenon from occurring [23,31,34].

Fig. 6a–c shows SEM images of the three multilayered films after they had been subjected to a cyclic bending test: PI/ZnO/ITO (150 nm), PI/ZnO/ITO (50 nm)/AgNW, and PI/AgNW. For all tests, the bending radius, R_b, was 3 mm. After $N = 7$ cycles, the sheet resistance of the PI/ZnO/ITO (150 nm) film increased sharply owing to the brittleness of the ITO layer (see Fig. 6d). However, the sheet resistance of the PI/ZnO/ITO (50 nm)/AgNW sample increased only slightly. This small increase in R_s can be attributed to the fact that the AgNWs did not break even after the failure of the ITO layer after 70 cycles of bending. Finally, the SEM image of the PI/AgNW film after $N = 2000$ cycles (see Fig. 6c) does not indicate any deterioration. Thus, the results of the bending tests confirmed that the supersonically sprayed AgNW films were mechanically resilient and can thus may employable as supplements or even replacements for the ITO layer. Thus, forming both a thin layer of ITO, which allows for the efficient transport of electrons, and a flexible AgNW layer can be a promising multilayer approach for the realization of flexible opto-electronic devices [35].

4. Conclusions

Transparent and conducting films of AgNWs were supersonically sprayed on flexible PI substrates on which ZnO and ITO layers had already been deposited. ZnO and ITO layers enhance surface electron transport in solar cells but limit device flexibility. Thus, transparent and conducting AgNW films were explored as potential substitutes. The effects of the deposition pressure (P_0) and temperature (T_0), which determined the impact velocity of the AgNWs on the substrate, were studied in detail. It was observed that, for $R_s \leq 30$ Ω/sq, the effect of the deposition pressure was minimal. However, for $R_s > 30$ Ω/sq, a lower P_0 value is preferable for obtaining films with higher transmittance and lower sheet resistance. On the other hand, for the films deposited at $P_0 = 4$ bar, the FoM value was highest for all n values. When T_0 was excessively increased, the air velocity (V_e) correspondingly increased, which produced unwanted bow shocks and thus prevented the efficient deposition of the AgNWs. Therefore, it is advised not to exceed $T_0 = 200$ °C, which would significantly sacrifice the sheet resistance of the films.

Acknowledgement

This research was supported by the Technology Development Program to Solve Climate Changes of the National Research Foundation (NRF) funded by the Ministry of Science, ICT and Future Planning (NRF-2016M1A2A2936760). This research was also supported by NRF-2013M3A6B1078879, NRF-2017R1A2B4005639, and NRF-2013R1A5A1073861.

References

[1] G.H. Gelinck, H.E.A. Huitema, E. van Veenendaal, E. Cantatore, L. Schrijnemakers, J.B. van der Putten, T.C. Geuns, M. Beenhakkers, J.B. Giesbers, B.-H. Huisman, Flexible active-matrix displays and shift registers based on solution-processed organic transistors, Nat. Mater. 3 (2004) 106–110.
[2] T. Sekitani, U. Zschieschang, H. Klauk, T. Someya, Flexible organic transistors and circuits with extreme bending stability, Nat. Mater. 9 (2010) 1015–1022.
[3] J.-S. Park, T.-W. Kim, D. Stryakhilev, J.-S. Lee, S.-G. An, Y.-S. Pyo, D.-B. Lee, Y.G. Mo, D.-U. Jin, H.K. Chung, Flexible full color organic light-emitting diode display on polyimide plastic substrate driven by amorphous indium gallium zinc oxide thin-film transistors, Appl. Phys. Lett. 95 (2009), 013503.
[4] J.-W. Lim, D.-Y. Cho, K. Eun, S.-H. Choa, S.-I. Na, J. Kim, H.-K. Kim, Mechanical integrity of flexible Ag nanowire network electrodes coated on colorless PI substrates for flexible organic solar cells, Sol. Energy Mater. Sol. Cells 105 (2012) 69–76.

[5] F. Kessler, D. Rudmann, Technological aspects of flexible CIGS solar cells and modules, Sol. Energy 77 (2004) 685–695.
[6] A. Chirila, S. Buecheler, F. Pianezzi, P. Bloesch, C. Gretener, A.R. Uhl, C. Fella, L. Kranz, J. Perrenoud, S. Seyrling, Highly efficient Cu(In,Ga)Se_2 solar cells grown on flexible polymer films, Nat. Mater. 10 (2011) 857.
[7] X. Wang, L. Zhi, N. Tsao, Ž. Tomović, J. Li, K. Müllen, Transparent carbon films as electrodes in organic solar cells, Angew. Chem. Int. Ed. 47 (2008) 2990–2992.
[8] F.L. Wong, M.K. Fung, S.W. Tong, C.S. Lee, S.T. Lee, Flexible organic light-emitting device based on magnetron sputtered indium-tin-oxide on plastic substrate, Thin Solid Films 466 (2004) 225–230.
[9] Z. Wu, Z. Chen, X. Du, J.M. Logan, J. Sippel, M. Nikolou, K. Kamaras, J.R. Reynolds, D.B. Tanner, A.F. Hebard, A.G. Rinzler, Transparent, conductive carbon nanotube films, Science 305 (2004) 1273–1276.
[10] L. Hu, D.S. Hecht, G. Gruner, Carbon nanotube thin films: fabrication, properties, and applications, Chem. Rev. 110 (2010) 5790–5844.
[11] J.-Y. Lee, S.T. Connor, Y. Cui, P. Peumans, Solution-processed metal nanowire mesh transparent electrodes, Nano Lett. 8 (2008) 689–692.
[12] S. De, T.M. Higgins, P.E. Lyons, E.M. Doherty, P.N. Nirmalraj, W.J. Blau, J.J. Boland, J.N. Coleman, Silver nanowire networks as flexible, transparent, conducting films: extremely high DC to optical conductivity ratios, ACS Nano 3 (2009) 1767–1774.
[13] X. Wang, L. Zhi, K. Müllen, Transparent, conductive graphene electrodes for dye-sensitized solar cells, Nano Lett. 8 (2008) 323–327.
[14] H.A. Becerril, J. Mao, Z. Liu, R.M. Stoltenberg, Z. Bao, Y. Chen, Evaluation of solution-processed reduced graphene oxide films as transparent conductors, ACS Nano 2 (2008) 463–470.
[15] W. Gaynor, J.-Y. Lee, P. Peumans, Fully solution-processed inverted polymer solar cells with laminated nanowire electrodes, ACS Nano 4 (2010) 30–34.
[16] Z. Yu, Q. Zhang, L. Li, Q. Chen, X. Niu, J. Liu, Q. Pei, Highly flexible silver nanowire electrodes for shape-memory polymer light-emitting diodes, Adv. Mater. 23 (2011) 664–668.
[17] J. Lee, P. Lee, H. Lee, D. Lee, S.S. Lee, S.H. Ko, Very long Ag nanowire synthesis and its application in a highly transparent, conductive and flexible metal electrode touch panel, Nanoscale 4 (2012) 6408–6414.
[18] D.-S. Leem, A. Edwards, M. Faist, J. Nelson, D.D.C. Bradley, J.C. de Mello, Efficient organic solar cells with solution-processed silver nanowire electrodes, Adv. Mater. 23 (2011) 4371–4375.
[19] F. Xu, Y. Zhu, Highly conductive and stretchable silver nanowire conductors, Adv. Mater. 24 (2012) 5117–5122.
[20] Y. Ahn, Y. Jeong, Y. Lee, Improved thermal oxidation stability of solution-processable silver nanowire transparent electrode by reduced graphene oxide, ACS Appl. Mater. Interfaces 4 (2012) 6410–6414.
[21] T.-G. Chen, B.-Y. Huang, H.-W. Liu, Y.-Y. Huang, H.-T. Pan, H.-F. Meng, P. Yu, Flexible silver nanowire meshes for high-efficiency microtextured organic-silicon hybrid photovoltaics, ACS Appl. Mater. Interfaces 4 (2012) 6857–6864.
[22] S. Ye, A.R. Rathmell, Z. Chen, I.E. Stewart, B.J. Wiley, Metal nanowire networks: the next generation of transparent conductors, Adv. Mater. 26 (2014) 6670–6687.
[23] J.-G. Lee, D.-Y. Kim, J.-H. Lee, S. Sinha-Ray, A.L. Yarin, M.T. Swihart, D. Kim, S.S. Yoon, Production of flexible transparent conducting films of self-fused nanowires via one-step supersonic spraying, Adv. Funct. Mater. 27 (2017). 1602548-n/a.
[24] J.A. Spechler, K.A. Nagamatsu, J.C. Sturm, C.B. Arnold, Improved efficiency of hybrid organic photovoltaics by pulsed laser sintering of silver nanowire network transparent electrode, ACS Appl. Mater. Interfaces 7 (2015) 10556–10562.
[25] Z. Yin, S. Wu, X. Zhou, X. Huang, Q. Zhang, F. Boey, H. Zhang, Electrochemical deposition of ZnO nanorods on transparent reduced graphene oxide electrodes for hybrid solar cells, Small 6 (2010) 307–312.
[26] D.-H. Cho, Y.-D. Chung, K.-S. Lee, N.-M. Park, K.-H. Kim, H.-W. Choi, J. Kim, Influence of growth temperature of transparent conducting oxide layer on Cu (In, Ga) Se 2 thin-film solar cells, Thin Solid Films 520 (2012) 2115–2118.
[27] Y. Ren, M. Baba, Y. Oishi, Preparation and characterization of organic thin films on substrates and self-supporting films by rf sputtering of polyimide films, Jpn. J. Appl. Phys. 44 (2005) 1987.
[28] H. Kim, C. Gilmore, A. Pique, J. Horwitz, H. Mattoussi, H. Murata, Z. Kafafi, D. Chrisey, Electrical, optical, and structural properties of indium–tin–oxide thin films for organic light-emitting devices, J. Appl. Phys. 86 (1999) 6451–6461.
[29] X. Cheng, H. Zhao, L. Huo, S. Gao, J. Zhao, ZnO nanoparticulate thin film: preparation, characterization and gas-sensing property, Sens. Actuators B Chem. 102 (2004) 248–252.
[30] J.-G. Lee, J.-H. Lee, S. An, J.Y. Yoon, J.-W. Choi, M.G. Kang, J.I. Lee, H.-e. Song, S.S. Al-Deyab, S.C. James, Effects of impact conditions on the electrical and mechanical properties of supersonic cold sprayed Cu–Ni electrodes, J. Alloys Compd. 695 (2017) 3714–3721.
[31] M.-W. Lee, J.-J. Park, D.-Y. Kim, S.S. Yoon, H.-Y. Kim, S.C. James, S. Chandra, T. Coyle, Numerical studies on the effects of stagnation pressure and temperature on supersonic flow characteristics in cold spray applications, J. Therm. Spray Technol. 20 (2011) 1085–1097.
[32] M. Lee, D. Kang, N. Kim, H. Kim, S. James, S. Yoon, A study of ejection modes for pulsed-DC electrohydrodynamic inkjet printing, J. Aerosol Sci. 46 (2012) 1–6.
[33] D.-Y. Kim, J.-J. Park, J.-G. Lee, D. Kim, S.J. Tark, S. Ahn, J.H. Yun, J. Gwak, K.H. Yoon, S. Chandra, Cold spray deposition of copper electrodes on silicon and glass substrates, J. Therm. Spray Technol. 22 (2013) 1092–1102.
[34] J. Pattison, S. Celotto, A. Khan, W. O'neill, Standoff distance and bow shock phenomena in the Cold Spray process, Surf. Coat. Technol. 202 (2008) 1443–1454.
[35] C.H. Chung, T.B. Song, B. Bob, R. Zhu, H.S. Duan, Y. Yang, Silver nanowire composite window layers for fully solution-deposited thin-film photovoltaic devices, Adv. Mater. 24 (2012) 5499–5504.
[36] S. Bae, H. Kim, Y. Lee, X. Xu, J.-S. Park, Y. Zheng, J. Balakrishnan, T. Lei, H.R. Kim, Y.I. Song, Roll-to-roll production of 30-inch graphene films for transparent electrodes, Nat. Nanotechnol. 5 (2010) 574–578.
[37] S. De, P.J. King, P.E. Lyons, U. Khan, J.N. Coleman, Size effects and the problem with percolation in nanostructured transparent conductors, Acs Nano 4 (2010) 7064–7072.
[38] D.Y. Kim, S. Sinha-Ray, J.J. Park, J.G. Lee, Y.H. Cha, S.H. Bae, J.H. Ahn, Y.C. Jung, S.M. Kim, A.L. Yarin, Self-healing reduced graphene oxide films by supersonic kinetic spraying, Adv. Funct. Mater. 24 (2014) 4986–4995.